https://doi.org/10.4322/2176-1523.20191685

CARACTERIZAÇÃO ELÉTRICA E ESTRUTURAL DA CERÂMICA DE CHUMBO E COBRE

Vander Alkmin dos Santos Ribeiro [1]
Adhimar Flávio Oliveira [2]
Rero Marques Rubinger [2]
Claudiney de Sales Pereira Mendonça [2]
Valesca Donizete de Oliveira [2]
Manoel Ribeiro da Silva [2]

Resumo

As cerâmicas de chumbo e cobre são materiais tecnicamente importantes devido à sua alta permeabilidade magnética, baixas perdas e alta resistividade. Neste manuscrito, apresentamos a produção de um conjunto de amostras através do processo cerâmico, envolvendo reações de estado sólido e alta temperatura entre os óxidos constituintes, e a caracterização da cerâmica $Pb_x Cu_{1-x} Fe_2O_4$, visando a formação de uma estrutura do tipo espinélio com propriedades eletrônicas adequadas para o desenvolvimento de novos dispositivos e aperfeiçoamento dos atuais. Para a caracterização foram realizadas medidas de difração de raios-X, medidas elétricas em corrente alternada e contínua em função da temperatura e Microscopia eletrônica de varredura. A partir da difração de raios-X é determinado que as amostras possuem estrutura do tipo espinélio cúbico e tetragonal e das medidas elétricas que o principal mecanismo de transporte está limitado por uma barreira potencial entre os cristalitos.
Palavras-chave: Estrutura spinel; Barreira nos limites dos cristalitos; Cerâmica Pb-Cu.

ELECTRICAL AND STRUCTURAL CHARACTERIZATION OF LEAD AND COPPER CERAMICS

Abstract

Lead and copper ceramics are technologically important materials due to their high magnetic permeability, low losses and high resistivity. In this paper, we present the production of a set of samples through the ceramic process, involving solid state and high temperature reactions between the constituent oxides, and the characterization of $Pb_x Cu_{1-x} Fe_2O_4$ ceramics, aiming the formation of a spinel-like structure with electronic properties suitable for the production of new devices and improvements on the current ones. The characterization measurements considered X-ray diffraction, electrical measurements in alternating current and continuous as a function of temperature and Scanning Electron Microscopy. From the X-ray diffraction it is determined that the samples have cubic and tetragonal spinel type structure and from the electrical measurements that the main transport mechanism is limited by a potential barrier among the crystallites.
Keywords: Spinel structure; Barrier at crystallite boundaries; Pb-Cu ceramics.

1 INTRODUCTION

Lead and copper ceramics are technologically important materials due to its soft magnetic materials with low magnetic coercivity, high saturation magnetization, high Curie temperature, low remanance, high electrical resistivity characteristics and high dielectric constant [1-3]. Materials with high dielectric constant are often used for various capacitors [4]. In microelectronics, high dielectric constant are useful especially as gate dielectrics in metal oxide semiconductor devices, mostly for transistors (MOSFETs) [5].

The spinel type ceramic are materials with the formula $M\ Fe_2O_4$, where M is a divalent metal ion. The oxygen atoms form a compact cubic structure with 64 tetrahedral sites and 32 octahedral sites with 8 out of 16 octahedral

[1] *Centro Universitário de Itajubá – FEPI, Itajubá, MG, Brasil. E-mail: vanderalkmin@gmail.com*
[2] *Universidade Federal de Itajubá – Unifei, Itajubá, MG, Brasil.*

2176-1523 © 2019 Associação Brasileira de Metalurgia, Materiais e Mineração. Published by ABM. This is an open access paper, published under the Creative Commons CC BY-NC-ND license (Attribution-NonCommercial-NoDerivs) - https://creativecommons.org/licenses/by-nc-nd/4.0/.

sites occupied by cations. A divalent cation tend to occupy the tetrahedral sites for the formation of a standard spinel structure, while a divalent cation occupy the octahedral sites forming an inverse spinel structure [6-8].

The electrical properties of the spinel type ceramics are primarily controlled by energy barriers that builds up between crystallites, due to the presence of trap states [9]. According to potential barrier between the crystallites model [10] the region between the crystallites consists of a large number of defects or impurities, which act as effective carrier traps. These defects or impurities migrate to the surface of the crystallites during the sintering process and accumulate at the crystallite boundaries. The defect or impurity is commonly associated to a deep level donor or acceptor. A coexistence of both donors and acceptors leads to a compensation of charge carriers by one of them, generating free positions for trapping free carriers from conduction and/or valence bands. This leads to a depletion of free carriers at the crystallite boundaries and a formation of ionized donors or acceptors known as space charge. Space charge builds up an electric field at crystallite boundaries that blocks the passage of charge carriers between crystallites.

Potential barrier between the crystallites model states that, when the trapping states in the region between the crystallites are ionized, they create a depletion region in the crystallite and a potential barrier at the interface [9,11]. This reduces the number of free carriers able to cross the potential barriers and transport current through the material. The effectiveness of this barrier depends on the space charge density which is dependent on the density of defects/impurities and the compensation ratio in these boundaries.

In this manuscript, we present the results of a set of samples of lead and copper ferrites. In addition, the electrical and structural characterizations of the sample set are presented, indicating that these have a crystalline structure of spinel type and have high resistivity under a large temperature change, due to the potential barrier between the crystallites, as will be described in the following sections.

2 MATERIALS AND METHODS

$Pb_xCu_{1-x}Fe_2O_4$ samples with x as a stoichiometry parameter assuming the values x = 0.00, 0.10, 0.20, were prepared by solid-state reaction using PbO, CuO and Fe_2O_3 (99.9% purity, Sigma-Aldrich). Initially, the oxides were weighted, considering the respective stoichiometry x and then grind in an agate mortar for about 1h. Using a uniaxial press the samples were compacted up to a pressure of 293 Mpa in the form of pellets of dimensions 7.5 mm diameter and 2.5 mm thickness and finally sintered at 1000Â°C for 6h at constant heating rate of 10°C/min in ambient air atmosphere.

X-ray diffraction patterns were performed using a diffractometer of type model X'pert Panalytical and identified with CuK α radiation in the 2θ range of 15° to 80° with a step size of 0.02° and counting time of 2 s. The identification of phases were carried out using the PDF2-ICDD database of software High Score Plus. The average crystallite size of the particles was determined by using the Debyeâ€“Scherrer formula [12]. The densities of the sintered samples were evaluated by the Archimedes method. The density of the water by Archimedes method used is 0.9983g/cm³ at the temperature of 19.5°C.

The samples were prepared by a sequence of grinding and polishing steps, followed by thermal etching at 930°C for 10 min. Scanning electron microscope (SEM) Zeiss brand, EVO MA15 model was used to investigate sample morphology with samples being gold sputtered before measurements. For the digital processing of the microscope image, the software program "analysis" (Soft Imaging System) is used.

The dc resistivity (ρ) of the samples was measured by two-probe standard method as a function of temperature. Due to high resistivity of samples, two probe methods is appropriate since thin disc shaped samples present lower resistance when compared to other geometries. Measurements were taken in the temperature range of 300 K to 725 K.

Impedance spectroscopy measurements were measured at room temperature using the software WinDETA by a Novo Control Technologies, model Apha-A high Performance Frequency Analyzer in the frequency range of 1Hz to 10MHz with drive voltage 1.0 Vrms and then the dielectric permittivity was calculated from fittings of impedance arcs considering the real part (Z') and imaginary part (-Z") of the complex impedance of the samples[19].

The sintering of poly-crystalline ceramics leads to the movement of excess ionic charges to the surface of crystallites and consequently the formation of potential barriers between them [10,13]. The potential between crystallites act as an energy barrier that limits the charge transport, defining the resistivity as by equation 1

$$\rho = \left[\frac{(2\pi m^* k_B T)^{1/2}}{Le^2 n}\right] \exp\left(\frac{E_b}{k_B T}\right) \quad (1)$$

here e is the electron charge, k_B the Boltzmann constant, T is the sample temperature, L is the average crystallite size, n is the free charge density, m* their effective mass and E_b the energy barrier is defined by:

$$E_b = \frac{L^2 e^2 N_d}{8\varepsilon\varepsilon_0} \quad (2)$$

where E_b is a constant and can be determined by a $\ln(\rho T^{-1/2})$ vs. 1000/T plot, N_d is the donor concentration and ε_0 is the vacuum permissivity and ε ï€ is the low frequency dielectric permittivity, determined by the impedance spectroscopy measurements.

The applicability of this model is tested by the Debye-length (L_D) given by Equation 3, i.e. if $L_D < L/2$, the activation energy is due to carrier trapping by ionized deep level defects at the crystallite boundaries [14,15].

$$L_D = \sqrt{\frac{k_B T \varepsilon \varepsilon_0}{e^2 N_d}} \quad (3)$$

The dielectric permittivity of all samples have been calculated considering a.c. capacitance measurements in the frequency range of 1 Hz to 10 MHz and Equation 4. In this equation, is the capacitance of the pellet, d is the thickness of the pellet, A is the cross-sectional area of the flat surface of the pellet [14,16,17].

$$\varepsilon = \frac{Cd}{\varepsilon_0 A} \quad (4)$$

3 RESULTS AND DISCUSSION

Figure 1 shows the X-ray diffraction patterns of samples. XRD pattern for sample with x = 0.00 indicates that it is formed exclusively by a cubic spinel structure (JCPDS 01-077-0010). The samples with x = 0.10 and x = 0.20 indicates that they are exclusively formed by the spinel phase with tetragonal spinel structure (JCPDS 34-0425) [18] and the formation of a second phase of the liquid phase of PbO [18].

The densities measured were 5.00 g/cm³ for x=0.00, 4.87 g/cm³ for x=0.10 and 4.66 g/cm³ for x=0.20, with a sintering temperature 1000°C for 6h. The relative density values (Apparent density / theoretical density) were greater than 86% consistent with the uniaxial pressing process for all samples. These results show that for all studied systems there was a good density of compaction.

In Figure 2 shows the results of the electrical measurement in DC performed in the samples of $Pb_xCu_{1-x}Fe_2O_4$, for x between 0.00 and 0.20. The resistivity measurements were carried out in the temperature range of 300 K to 725 K. In Figure 2 a high temperature, 1000/T : 1.7, a change in the conduction mechanism of the samples is observed. In this region, the change of slope indicates that the energy is enough for the carriers to tunnel between the crystallites. In the region between 350 K and 550 K a linear behavior was performed indicating that barriers in crystallite boundaries are present and that this model is applicable. Figure 2 shows the fittings as thin straight lines used to obtain an E_b, Equation 2, with respective values shown in Table 1.

The parameters that relate the electric conduction model to crystallites with potential barriers are presented in Table 1. In the first column shows the stoichiometric fraction, x, in the second the low frequency dielectric permittivity value, which was obtained through the fittings on

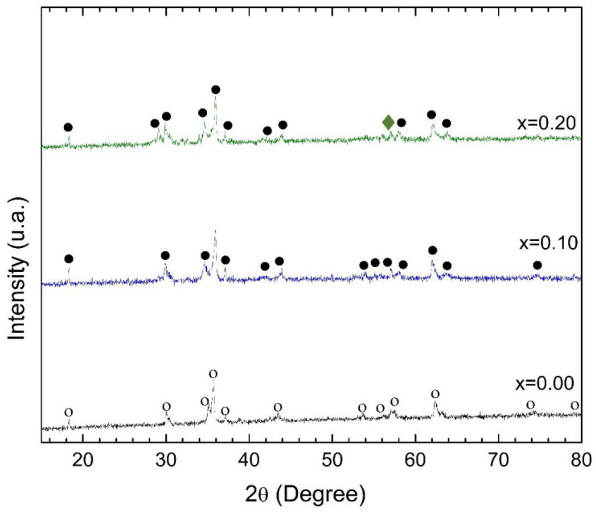

Figure 1. X-ray diffraction patterns of $Pb_xCu_{1-x}Fe_2O_4$. The stoichiometry x and plane indexes corresponding to peaks are indicated (◦) Cubic spinel (•) Tetragonal spinel (♦) PbO.

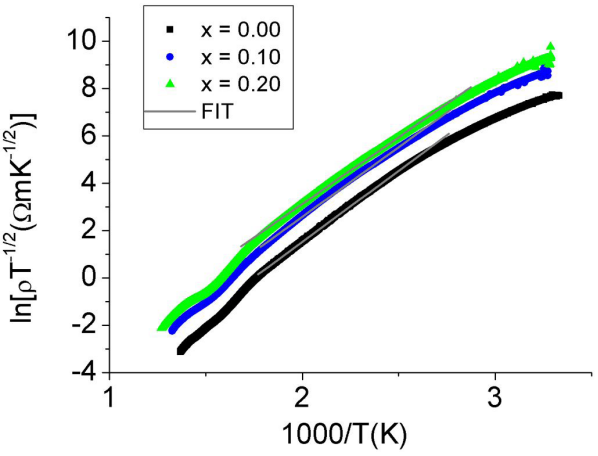

Figure 2. Temperature dependence of electrical resistivity plotted as $\ln(\rho\, T^{-1/2})$ vs (1000/T) $Pb_xCu_{1-x}Fe_2O_4$ samples with x = 0.00, 0.10 and 0.20. Barrier at crystallite boundaries plot and fittings at the linear range. In the caption, we present the symbols and colors (online) corresponding to the samples. Samples have barrier-limited conduction between 350K and 550K.

Table 1. Parameters of the barrier model for $Pb_xCu_{1-x}Fe_2O_4$ samples. x is the stoichiometric parameter, average crystallite size (L), the half of the average crystallite size (L/2), Debye screening Length (L_D). The last two columns are related to the ability of carriers to cross such barriers, i.e. Nd the donor concentration and Eb the energy barrier height

X	ε	L/2	L_D	N_D	E_b
		(nm)	(nm)	(10^{19} cm^{-3})	(eV)
0.00	153	29.86	2.86	3.82	0.50
.10	1088	25.15	2.32	530	0.49
.20	4694	36.53	3.61	137	0.47

the impedance measurements of the samples. The average value of crystallite size, $L/2$, was obtained through the Debye-Scherrer equation and the Debye screening Length, L_D, by Equation 3. In the fifth column, the values of donor concentration, NC, also obtained through the model and in the last column the value of Eb, obtained through the fittings on the graph of Figure 2, are presented. From the slopes of $\ln(\rho\, T^{-1/2})$ vs (1000/T) curves in Figure 2, the values of the energy barrier (E_b) have been calculated for samples and their values are given in Table 1. Then, determine the donor concentration values (N_D) using Equation 2 for investigated samples [9].

The samples with x = 0.00 to x = 0.20 meets the condition $L_D < L/2$ (L_D is the Debye screening length), i.e. energy barriers exist between the crystallites, due to the surface trap states. Figures 3 to 5 shows micrographs with magnification 25000X and 50000X for the lead-free sample (x = 0.00) to the sample with x = 0.20. The micrographs

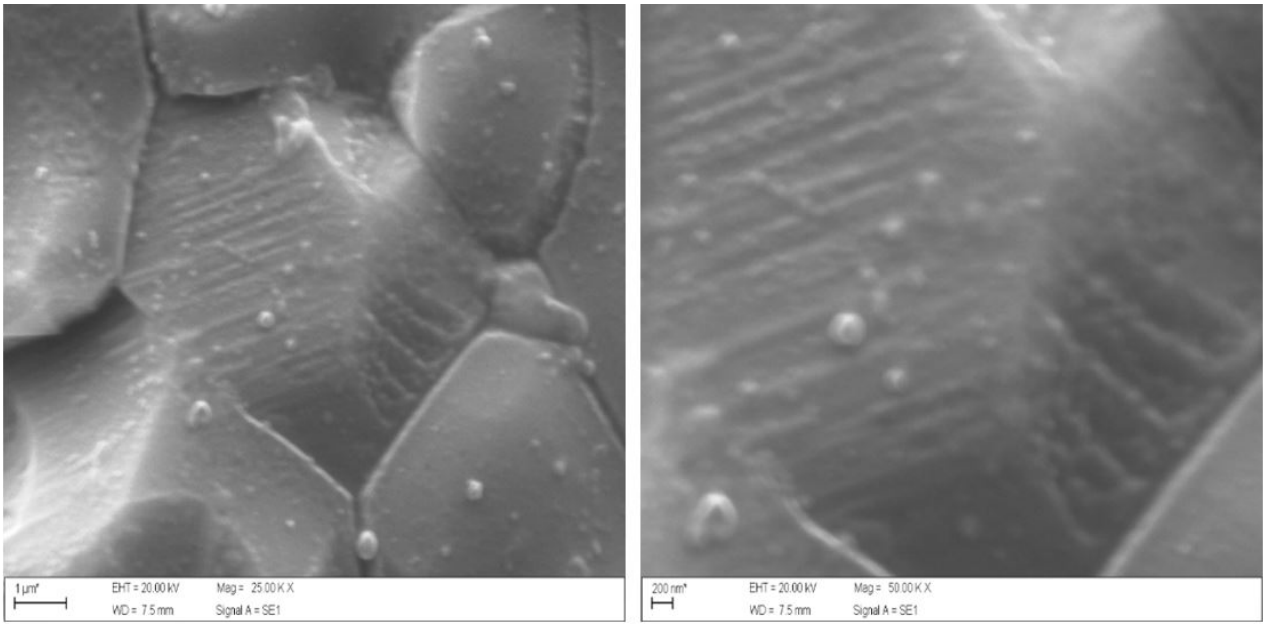

Figure 3. Micrograph of sample with x = 0.00. The right with magnification 25000X and the left with magnification 50000x.

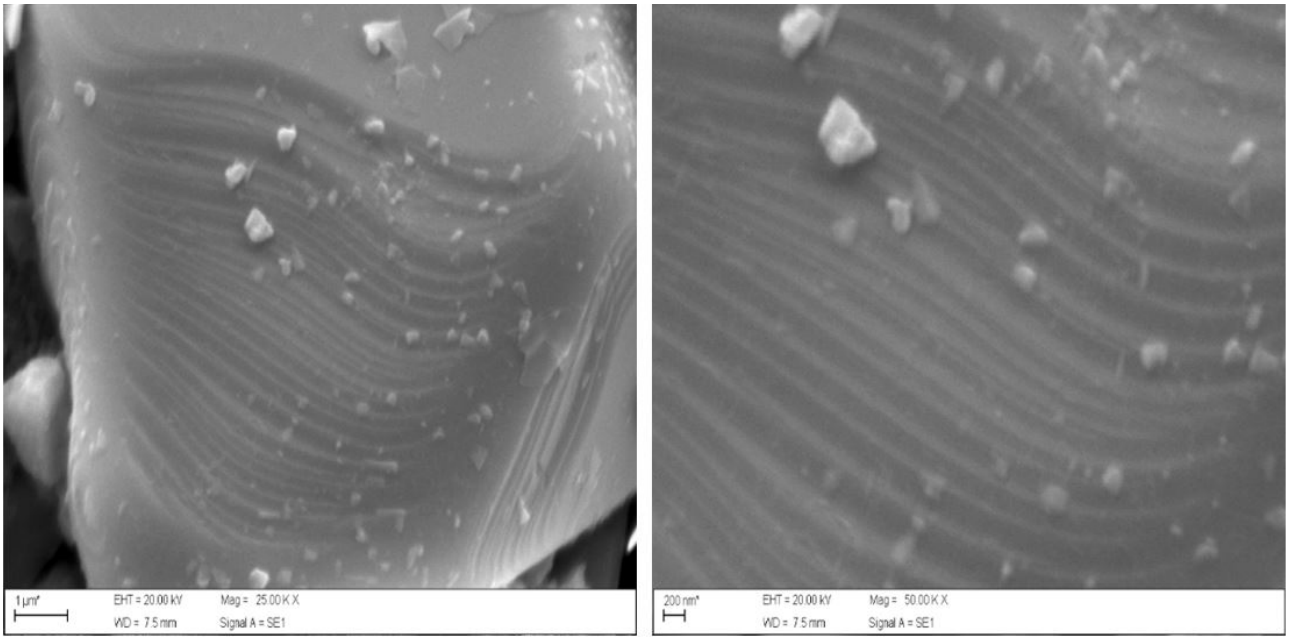

Figure 4. Micrograph of sample with x = 0.10. The right with magnification 25000X and the left with magnification 50000x.

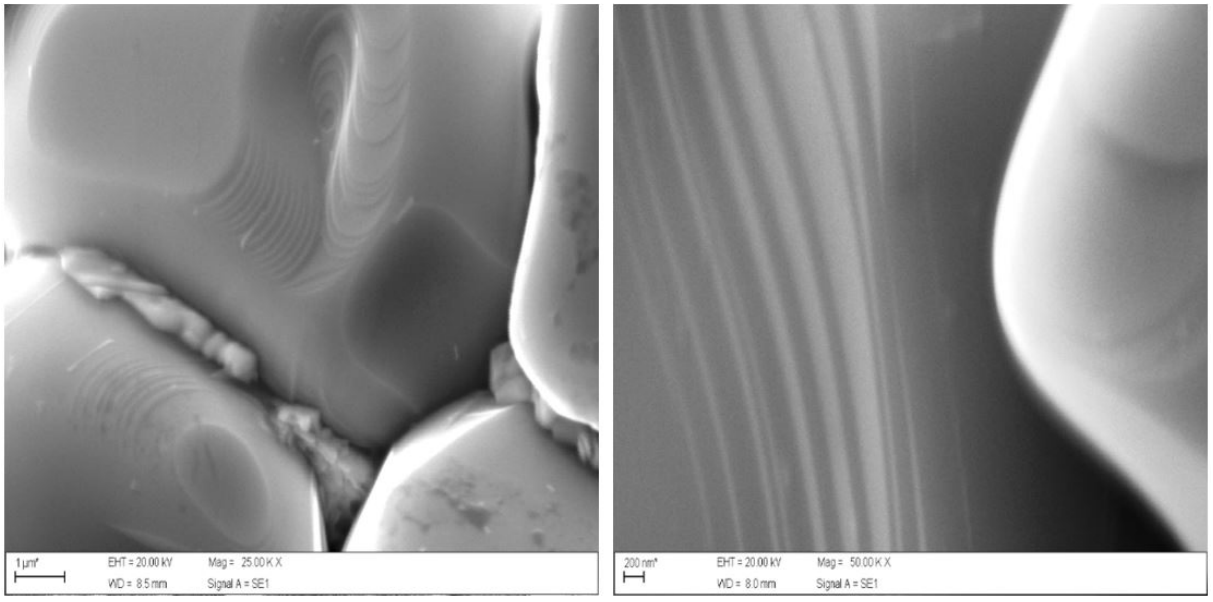

Figure 5. Micrograph of sample with x = 0.20. The right with magnification 25000X and the left with magnification 50000x.

clearly presents crystallites of varying size and orientation and irregular shaped platelet nanometer dimensions. Within each crystallite, atoms are arranged periodically, remaining with the same crystalline structure and may be considered as small isolated crystals.

A mixed nature of fractures occurs in this material, i.e. along boundaries as well as through grains. In the case of the lead and copper ceramics, the microstructure shows grain boundaries. Regions between adjacent grains are called grain boundary, in the case of materials with nanometric dimensions, or for materials with reduced dimensions, which are formed by mesoscopic particles. The grain boundary is a complex structure consisting of small layer of disoriented atoms, this is due to the fact that in this region a transition between different orientations in the vicinity of the grain occurs.

Thus, the grain boundary is a region where we can observe a decrease in frequency of the lattice, and characterized by a large number of defects caused by incomplete atomic bonds. With regard to electric conduction, the grain boundary region presents a low electron mobility compared with region between the crystallites. The electrical properties are mainly controlled when the traps states in the region between the crystallites are present, and the conductivity of material changes due to the capture of free carriers. Figures 4 and 5 show small crystallites usually joined at their surfaces via grain. The conductivity of polycrystalline materials is related to the potential barrier between the crystallite.

According to potential barrier between the crystallites model, in a polycrystal, the region between the grains presents a large number of defects, which act as effective carrier traps. This model states that, when the trapping states in grain region are unoccupied, they create a depletion region in the grain and a potential barrier at the interface. This reduces the number of free carriers available for electrical conduction [14]. The electrical transport in all of the investigated samples is related to charged impurities carrier scattering mechanism in the region between the grains [20].

It is also observed that in the sample with x = 0.20 the formation of a secondary phase occurred, which is evidenced in the X-ray diffractograms. Microstructure studies showed that oxide PbO (T_m = 888°C) forms a liquid phase on the grain boundaries [21].

4 CONCLUSION

The XRD analysis reveals for sample with x = 0.00 the formation of a single-phase cubic spinel structure and for x = 0.10 and x = 0.20 the formation of a single phase of tetragonal spinel structure. The resistivity decreases with increasing temperature showing semiconductor behavior. The sample with x = 0 to x = 0.20 meets the condition $L_D < L/2$ and energy barriers are formed with an energy about half an eV between the grains region, due to the surface trap states. Such characteristics make lead ceramics and copper a material with great potential in devices that need high electrical resistivity and high dielectric constant. These materials are often used for various capacitors. In microelectronics, high dielectric constant are useful especially as gate dielectrics in metal oxide semiconductor devices, mostly for transistors (MOSFETs).

Acknowledgements

We acknowledge support from the Brazilian Institutions CNPq, CAPES, and FAPEMIG.

REFERENCES

1 Gaikwad VB, Gaikwad SS, Nikam RD. Synthesis and characterization of nano-crystalline Cu and Pb. Sensors and Transducers. 2011;134:132-142.

2 Costa ACFM, Tortella E, Morelli MR, Kiminami RHGA. Synthesis, microestruture and magnetic properties of Ni-ZnFerrites doped with copper. Journal of Magnetism and Magnetic Materials. 2003;256:174-182.

3 Askeland DR, Fulay PP, Wright WJ. The science and engineering of materials. 6th ed. USA: CL Engineering; 2010.

4 Sakabe Y, Minai K, Wakino K. High-dielectric constant ceramics for base metal monolithic capacitors. Japanese Journal of Applied Physics. 1981;20:147-150.

5 Nalwa HS. Handbook of low and high dielectric constant materials and their applications. Vol. 2. USA: Academic Press; 1999.

6 Torquato RA, Portela FA, Gama L, Cornejo DR, Rezende SM, Kiminami RHGA, et al. Avaliação da microestrutura e das propriedades magnéticas de ferritas Ni-Zn dopadas com cobre. Cerâmica. 2008;54:55-62.

7 Hoque SM, Samirullah M, Khan FA, Hakim MA, Saha DK. Structural and magnetic properties of Li-Cu mixed spinel ferrites. Physica B. Physics of Condensed Matter. 2011;406:1799-1804.

8 Wei QM, Li JB, Chen YJ, Han YS. X ray study of cation distribution in NiMn1-xFe2-xO4. Materials Characterization. 2001;47:247-252.

9 Yildiz A, Serin N, Kasap M, Serin T, Mardare D. The thickness effect on the electrical conduction mechanism in titanium oxide thin films. Journal of Alloys and Compounds. 2010;493:227-232.

10 Preis W, Sitte W. Electrical properties of grain boundaries in interfacially controlled functional ceramics. Journal of Electroceramics. 2015;34:185-206.

11 Mancini MW, Paulin PI Fo. Potential barriers mapping by atomic force microscopy in lanthanum doped BaTiO3 based ceramics. Cerâmica. 2007;53:147-152.

12 Maria KH, Choudhury S, Hakim MAH. Structural phase transformation and hysteresis behavior of Cu-Zn ferrites. International Nano Letters. 2013;42:1-10.

13 Oliveira VD, Rubinger RM, Silva MR, Oliveira AF, Rodrigues G, Ribeiro VAS. Magnetic and Electrical Properties of MnxCu1-xFe2O4 Ferrite. Materials Research. 2016;19:786-790.

14 Ribeiro VAS, Rubinger RM, Oliveira AF, Mendonça CSP, Silva MR. Magnetic properties and potential barrier between crystallites model of MgGa2-xFexO4 ceramics. Cerâmica. 2016;62:365-369.

15 Mardare D, Iftimie N, Crisan M, Raileanu M, Yildiz A, Coman T, et al. Electrical conduction mechanism and gas sensing properties of Pd-doped TiO2 films. Journal of Non-Crystalline Solids. 2011;357:1774-1779.

16 Barsoukov E, Macdonald JR. Impedance spectroscopy: theory, experiment, and applications, 2nd ed. USA: Wiley; 2005.

17 Macdonald JR. Impedance spectroscopy. Annals of Biomedical Engineering. 1992;20:289-305.

18 Sridhar R, Ravinder D, Kumar KV. Properties of copper substituted nickel nano-ferrites. International Journal of Engineering Research and Applications. 2013;3:2021-2024.

19 Mocanu ZV, Apachitei G, Padurariu L, Tudorache F, Curecheriu LP, Mitoseriu L. Impedance spectroscopy method for investigation of the polycrystalline inhomogeneous ceramics. The European Physical Journal Applied Physics. 2011;56:10102.

20 Ravinder D, Reddy KS, Mahesh P, Rao TB, Venudhar YC. Electrical conductivity of chromium substituted copper ferrites. Journal of Alloys and Compounds. 2004;370:L17-L22.

21 Mirzaee O. Influence of PbO and TiO2 additives on the microstructure development and magnetic properties of Ni–Zn soft ferrites. Journal of King Saud University - Engineering and Sciences. 2013;26(2):152-158.

Received: 09 Mar. 2018
Accepted: 15 Mar. 2019